Fibrillar Structure in Aqueous Methylcellulose Solutions and Gels

ARTICLE *in* MACROMOLECULES · DECEMBER 2013

Impact Factor: 5.8 · DOI: 10.1021/ma4021642

Macromolecules

Article

pubs.acs.org/Macromolecules

Fibrillar Structure in Aqueous Methylcellulose Solutions and Gels

Joseph R. Lott,[†] John W. McAllister,[†] Matthew Wasbrough,[‡,⊥] Robert L. Sammler,[§] Frank S. Bates,*[,∥] and Timothy P. Lodge*[,†,∥]

[†]Department of Chemistry, University of Minnesota, Minneapolis, Minnesota 55455, United States

[‡]National Institute of Standards and Technology, Gaithersburg, Maryland 20899-1070, United States

[⊥]Department of Chemical and Biomolecular Engineering, University of Delaware, Newark, Delaware 19716, United States

[§]Materials Science and Engineering, The Dow Chemical Company, Midland, Michigan 48674, United States

[∥]Department of Chemical Engineering & Materials Science, University of Minnesota, Minneapolis, Minnesota 55455, United States

Supporting Information

ABSTRACT: The fibrillar structure of aqueous methylcellulose (MC) gels was probed using a combination of small-angle neutron scattering (SANS), ultra-small-angle neutron scattering (USANS), and cryogenic transmission electron microscopy (cryo-TEM). The effect of molecular weight (M_w) and concentration on the gel structure was explored. The fibrillar morphology was consistently observed at elevated temperatures (≥70 °C), independent of concentration and M_w. Moreover, the fibril dimensions extracted from SANS by fitting to a scattering function for semiflexible cylinders with disperse radii revealed that the fibril diameter of ca. 14 ± 1 nm is constant for a mass fraction range of 0.01%−3.79% and for all M_w investigated (49−530 kg/mol). Comparison of the measured SANS curves with predicted scattering traces revealed that at 70 °C the fibrils contain an average volume fraction of 40% polymer. Taking linear combinations of low temperature (solution state) and high temperature (gel state) SANS traces, the progression of fibril growth with temperature for aqueous MC materials was determined. At low temperatures (≤30 °C) no fibrils are present, whereas in the vicinity of 40−50 °C a small fraction begins to form. For temperatures ≥70 °C, virtually all of the chains are incorporated into the fibrillar structure. The persistence of the fibril structure during cooling was probed by SANS and cryo-TEM. The well-established rheological hysteresis upon cooling is directly correlated to the persistence of the fibril structures. Furthermore, cryo-TEM images taken upon heating to 50 °C showed no fibrils, whereas images for samples that were first heated to 70 °C and then cooled to 50 °C clearly display the fibrillar structure. USANS measurements revealed that heterogeneities in the gels persist beyond the largest length scale accessed in scattering experiments (~20 μm), consistent with the observed optical turbidity.

INTRODUCTION

Cellulose is the most abundant polymer on Earth. As such, many methods to utilize this plentiful resource have been developed. Among them, chemical modification reactions give rise to an array of useful materials. For the class of polymers labeled cellulose ethers (CEs), some hydroxyl groups native to the glucose rings of the polymer backbone are substituted with alkoxy moieties. Cellulose ethers receive continued attention because they have many characteristics that resonate with the concepts of green chemistry; they are derived from natural resources, nontoxic, biodegradable, and *generally recognized as safe* by the US Food and Drug Administration. Methylcellulose (MC) enjoys significant commercial interest and is primarily employed in food applications and in a wide array of commodity products ranging from building materials to pharmaceuticals and personal care formulations. MC exhibits lower critical solution temperature (LCST) phase behavior in aqueous systems; at low temperatures the polymer is soluble, while sufficiently concentrated solutions will gel at elevated temperatures. Recently, we reported the structure of aqueous MC gels in both real (cryogenic transmission electron microscopy, cryo-TEM) and reciprocal space (small-angle neutron scattering, SANS), using a polymer with $M_w \approx 300$ kg/mol.[1] In the solution state, no pronounced structures were found, and the samples could be considered typical semidilute, entangled, semiflexible polymer solutions. At elevated temperatures (i.e., gel state) a fibrillar structure was found to persist over sample-spanning length scales with a consistent fibrillar diameter of ca. 15 nm that was independent of polymer concentration for mass fractions over the range of 0.09%−2.45%.

For a system that has been studied in the literature since the early 1900s,[2,3] although the existence of fibrils has been previously suggested,[1,4−7] this definitive revelation of a fibrillar

Received: October 21, 2013
Revised: November 26, 2013
Published: December 11, 2013

gel structure represents a paradigm shift in how these gels are conceptualized. However, given the propensity of native cellulose to form fibrils,[8] the fibrillar structure of MC gels is perhaps less surprising in retrospect. Fibrillar gels[9] are also formed by a diverse range of chemical species such as actin,[10] tubulin,[11,12] keratin,[13,14] collagen,[15,16] and agarose[17] as well as synthetic polymers including poly(vinyl chloride),[18] isotactic poly(styrene),[19] stereoregular poly(methyl methacrylate),[20] poly(styrene)−poly(isocyanodipeptide) block copolymers,[21] and poly(3-hexylthiophene).[22] Small molecule gelators can also self-assemble to form fibrillar gels.[23] Fibrillar networks are ubiquitous in natural systems, playing vital roles in living organisms such as the function of the cytoskeleton,[24] blood clotting,[25] and the development of Alzheimer's disease.[26] As such, there is a growing body of literature related to the mechanical properties of fibrillar networks and their response to deformation.[27−35] Such a treatment, correctly applied to MC, could lead the way to a revised understanding of the widely reported rheological behavior of MC and guide efforts in the design of novel materials. However, in order to utilize these treatments, knowledge of the parameters describing the fibril network (persistence length, fibril density, fibril diameter) is required. Therefore, quantification of the nature of the fibrillar structure for MC gels is not only an important fundamental inquiry into the nature of MC, but also critical for expanding insight into the mechanical properties of MC gels.

The most prevalent methods for direct investigation of the structure of MC gels have been scattering techniques. Given that MC solutions form turbid gels, scattering methods employing visible light are of limited utility, so small-angle X-ray (SAXS) and SANS are advantageous experimental approaches. Several studies have explored the effects of temperature and concentration on the scattering from MC gels and solutions.[36−38] Similar behavior is observed, and while the data qualitatively agree with one another, there has not been a consistent treatment of the scattering data for MC gel systems. The behavior generally observed across most SAXS and SANS experiments is featureless, low intensity scattering at low temperatures (∼25 °C), whereas at elevated temperatures, in the gel state, scattering intensity increases by several orders of magnitude, especially at lower wavevectors. For the gel state, various treatments of the data have reported a structural feature corresponding to a radius of ∼5−8 nm.[36−38] However, the scattering data were not interpreted within the context of the fibrillar gel structure revealed by recent cryo-TEM experiments.[1,6,7] These well-defined cryo-TEM experiments are so compelling that the previous fibril-free interpretation of SANS length scales, presented by some of us,[36,38] should be superseded by the present work.

In this study, we utilize SANS to provide detailed insight into the structure of MC materials, while varying M_w and concentration. Detailed modeling of the SANS curves allows for the determination of the composition of the individual fibrils in the gel state as well as the partitioning of chains between free and fibrillar states as the sample transverses the sol−gel transition. Cryogenic transmission electron microscopy confirms the presence of fibrils and, crucially, reveals that well-established hysteresis in rheology[3,4,6,36,39,40] is directly correlated to hysteresis in fibril growth and dissolution. In addition, ultrasmall-angle neutron scattering (USANS) experiments allow for examination of the larger scale features of the gels.

EXPERIMENTAL SECTION

Sample Preparation. All methylcellulose materials were provided by The Dow Chemical Company. These commercial-grade materials are sold under the trade name of METHOCEL brand cellulose ethers. These five materials were selected for their similar average degree of substitution (1.8 ≤ DS ≤ 1.9 mol CH_3O/mol anhydroglucose unit, AGU) and contrasting weight-average molecular weights M_w (49, 150, 300, 400, and 530 kg/mol). Four of these MC materials are denoted solely by their molecular weights (MC49, MC150, MC300, and MC530). They are known to have similar gel temperatures at any given MC concentration in water.[40] One further material, denoted MC400S, is prepared by a different commercial process[41] designed to produce water-soluble MC materials with lower gel temperatures, and higher hot gel moduli, even though their key average coarse-grained metrics (DS and M_w) of chemical structure are similar to the other four materials. All aqueous solutions were prepared and hydrated by a hot/cold process as previously reported.[40]

Transmission Electron Microscopy. Vitrified samples were prepared with the aid of an FEI Vitrobot Mark III automated vitrification device. Cold aqueous MC solutions were filtered through 0.45 μm syringe filters into small vials. The vials were heated in an oil bath at the desired temperature for 30 min and then rapidly applied to the TEM grid (with a lacey carbon support mesh) within the Vitrobot environmental chamber, which was set at the corresponding temperature and 100% relative humidity. The gels were vitrified by rapid plunging into a pool of liquid ethane, cooled with liquid nitrogen. Vitrified samples were kept at cryogenic temperatures throughout the imaging process. TEM images were recorded using a FEI Technai Spirit BioTWIN transmission electron microscope in conjunction with an Eagle CCD camera. Images were obtained using an accelerating voltage of 120 kV, and the sample temperature was held at −179 °C. The working magnification range was between 16 000× and 25 000×.

Small-Angle Neutron Scattering (SANS). SANS measurements were performed at the National Institute for Science and Technology (NIST) on the NG7 30 m SANS instrument as well as Oak Ridge National Laboratories (ORNL) on the CG-2 SANS instrument at the HFIR. The q range accessed in a particular experiment was a function of the neutron wavelength (4.75 and 8.08 Å for ORNL and NIST, respectively) in conjunction with the detector distance (1−15 m) that allowed for data acquisition over a q range of 0.0009−0.3 $Å^{-1}$. Data were acquired for 3−90 min at each condition, depending on detector count rates. In all experiments, cold MC solutions (in D_2O) were filtered through 0.45 μm syringe filters into sample cells with a path length of 4 and 5 mm for NIST and ORNL, respectively. The samples were kept at 5 °C overnight prior to SANS experiments and heated to each desired discrete temperature, and the scattering was measured. The data were corrected for background and empty cell scattering as well as detector response. The 2D data were radially averaged using either NCNR or ORNL SANS reduction macros for WaveMetrics Igor Pro software to obtain $I(q)$ vs q plots.[42] To correct for incoherent scattering, for each scattering curve the high q data (0.15−0.30 $Å^{-1}$) were plotted as q^4I vs q^4, and the slopes of the resulting straight lines were subtracted from each point in the original $I(q)$ vs q data set. In all modeling, the data above q = 0.1 $Å^{-1}$ were ignored as it was outside the size range of interest, and the low intensities are prone to significant alteration during background correction.

Ultrasmall-Angle Neutron Scattering (USANS). USANS measurements were carried out at the National Institute of Science and Technology (NIST) on the BT5 perfect crystal diffractometer. Using a neutron wavelength of 2.4 Å (6% $\Delta\lambda/\lambda$), a q-range of 0.00003−0.0026 $Å^{-1}$ was accessed. Cold MC solutions were filtered through 0.45 μm syringe filters into NIST sample cells with a path length of 4 mm. The samples were kept at 5 °C overnight prior to SANS experiments and heated to each desired discrete temperature, and data were acquired for 7 h at each condition. The data were reduced and desmeared using the NIST-provided algorithms for WaveMetrics Igor Pro software.[42]

dx.doi.org/10.1021/ma4021642 | Macromolecules 2013, 46, 9760−9771

RESULTS

In our preliminary exploration of the structure of MC300 gels, we employed a combination of cryogenic transmission electron microscopy (cryo-TEM) and small-angle neutron scattering (SANS).[1] The cryo-TEM images revealed a fibrillar gel structure with a fibril diameter of 15 ± 2 nm, which was confirmed by fitting SANS curves to a form factor for semiflexible cylinders with polydisperse radii. This scattering model serves as the basis for the current study into the size and composition of MC gels for several M_w and therefore warrants more detailed consideration.

The model was developed by Pedersen and co-workers[43,44] and later enhanced by Chen et al.[45] and is summarized in eq 1.

$$I_{WC}(q, L, b, R_{CS}) = \phi_{cyl}(\Delta\rho)^2 S_{WC}(q, L, b) P_{CS}(q, R_{CS}) + BD \quad (1)$$

The operating principle is that since the contour length (L) of the cylinder is much greater than the radius of the cross section (R_{CS}), their respective contributions to the overall scattering (I_{WC}) can be decoupled into the product of longitudinal (S_{WC}) and cross-sectional terms (P_{CS}).[46] The scattered intensity as the scattering vector $q \to 0$, $I(0)$, is proportional to the product of the volume fraction of cylinders (ϕ_{cyl}) and the square of the contrast in scattering length density ($\Delta\rho$) between the cylinder and surrounding solvent. The longitudinal term is a scattering function based on the wormlike chain of Kratky and Porod,[47] in which excluded volume effects have been incorporated. There is no analytical solution for this scattering function, so Monte Carlo simulations were employed to arrive at a parametrized function. The radial term is based on the cross section of the cylinder and calculated using the scattering equation for a rigid rod.[45] A more complete summary of the model is presented in the Appendix.

Fibril Diameter. The previous investigation into the fibrillar MC gel structure examined a single M_w at multiple concentrations. In order to explore the universality of the fibril phenomenon, we first examined a set of four MC materials representing a wide range of M_w. Figure 1 displays SANS curves recorded from gels with equal concentrations but different M_w at 70 °C. (The differences in the q ranges of the individual traces are a result of different detector distances and neutron wavelengths employed during different experiments and across different facilities.) It has been previously reported that for MC with the same M_w SANS curves for gels superpose when the intensity is normalized by concentration.[1,36] This indicates that the gel structure is independent of the sample concentration. The same behavior (Figure S1) is observed for the data in Figure 1 for MC chains where M_w spans an order of magnitude and reveals that the fibril structure, for size scales ≤600 nm, does not depend on M_w. To aid in visualization, the curves in Figure 1, along with their best fits using eq 1, have been vertically shifted. All the traces scale as $I(q) \approx q^{-1.8}$ at low q, which is reflective of semiflexible fibrils in a good solvent.[5] For the lowest M_w sample, an upturn is observed at the lowest q values (*vide infra*). However, the $q^{-1.8}$ behavior is present from $0.003 \le q \le 0.015$ Å^{-1}. All SANS traces display a break in slope occurring near $q \approx 0.015$ Å^{-1}, a feature due to the size of the fibril cross section. Porod behavior with a slope of $\approx q^{-4.4}$ is found at higher q, indicative of a sharp interface between the fibril and the solvent. Equation 1 was found to quantitatively describe the scattering behavior across the entire q range. The values extracted for the cylinder radii, dispersity in radii, and Kuhn lengths are tabulated in Table S1; the radii are in excellent agreement with the previous cryo-TEM and SANS results, with diameters of ca. 14 ± 1 nm.

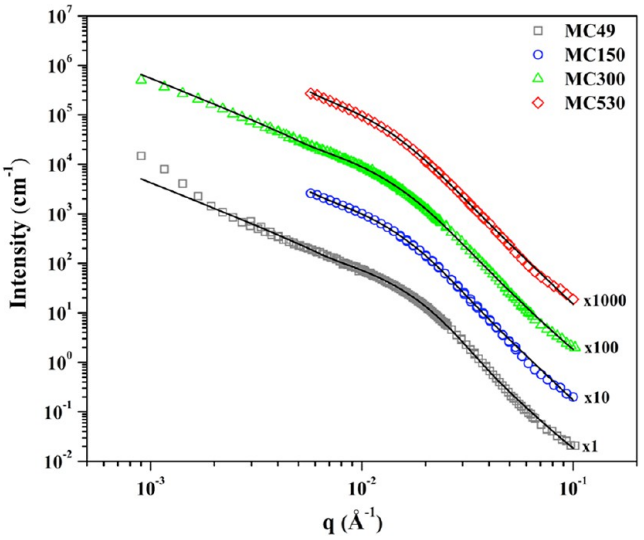

Figure 1. Scattering intensity versus scattering vector q at 70 °C for aqueous MC gels with a mass fraction of 1.36% and varying molecular weight. To aid in visualization, the traces have been vertically shifted by the factors indicated. Black lines are the best fits to eq 1, which have been shifted by the same factor as the respective data.

Effect of MC Preparation Method. Important additional factors that influence the behavior of MC materials are the spatial distribution and regiochemical distribution of the methoxy moieties. Much effort has been devoted to controlling the distribution of methoxy groups along the polymer backbone by employing homogeneous reaction conditions in the solution state,[48−51] or the position of methoxy groups on the individual anhydroglucose rings using regiospecific chemistries.[52−55] These factors can influence many aspects of MC behavior including gelation, solubility, and phase transitions.[48−55] However, the precise structure−property relationships are not well understood, nor is it clear if this leads to gel structures that are distinctly different than typical commercial MCs. To probe this idea, a commercial MC with a T_{gel} substantially (≈15 °C) lower than the other MC materials (at the same concentration) was investigated.[41] This low-T_{gel} material has a M_w within the range of the materials in Figure 1 and a matched DS. Given the commensurate M_w and that the overall stoichiometry of the methoxy substitution is equal, the obvious conjecture is to assign the difference in behavior to some difference in the spatial or regiochemical arrangement of the methoxy moieties. Precise measurement of such structural chemical details is challenging,[56,57] is an active area of research, and is beyond the scope of this paper.

As an initial method, cryo-TEM was employed to image the gel state. Figure 2a contains a cryo-TEM image for a MC400S sample with a mass fraction of 0.20% MC with the same DS and similar M_w as the MCs in Figure 1, but with a much lower T_{gel} (≈ 45 °C). Yet, the gel structure apparent in Figure 2a is very similar to what has been previously found for other MC materials.[1,6,7] The gel has a fibrillar network with heterogeneity on the scale of hundreds of nanometers. The fibril diameter is consistent along each fibril as well as among different fibrils and is 14 ± 2 nm in the image. SANS provides an excellent method to verify the dimensions of the fibrillar structure. Figure 2b contains SANS traces recorded at 70 °C for two concentrations

dx.doi.org/10.1021/ma4021642 | Macromolecules 2013, 46, 9760−9771

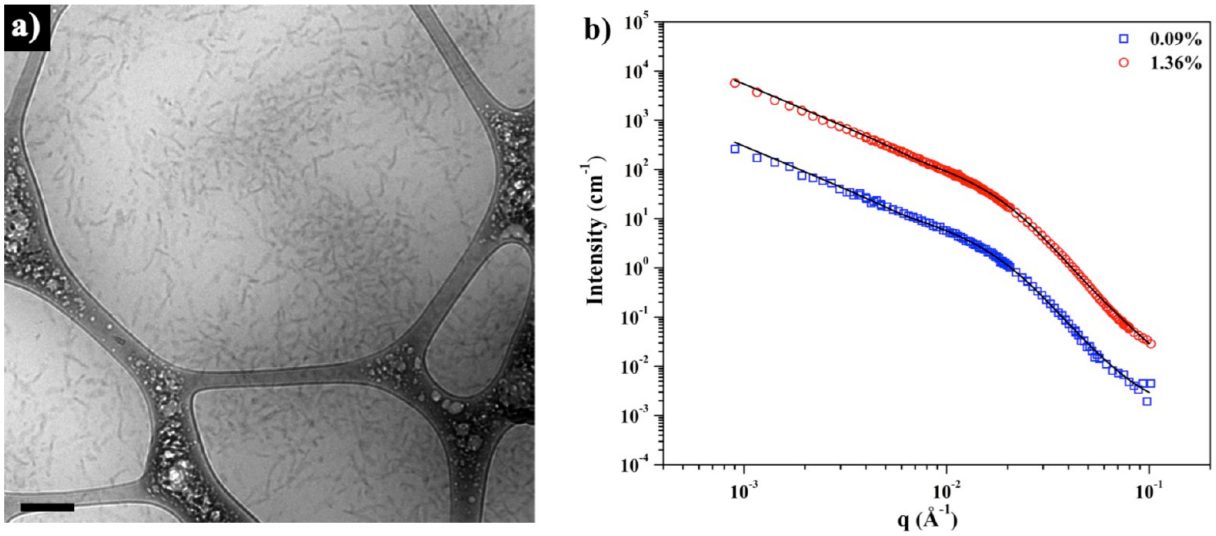

Figure 2. (a) Cryo-TEM image of a MC400S sample with a mass fraction of 0.20% vitrified from 65 °C on a lacey carbon support grid. The scale bar represents 200 nm. (b) Scattering intensity versus scattering vector q at 70 °C for aqueous MC400S gels with mass fractions of 0.09% (blue) and 1.36% (red). Black lines are the best fits to eq 1.

of MC400S. Qualitatively, the curves are very similar to those in Figure 1. Fitting the model to the data yields a slightly smaller fibril radius of 12 ± 1 nm with a dispersity of 0.5 at both concentrations. As is the case for typical commercial MCs, the SANS curves for the low-T_{gel} materials superpose with one another when the scattered intensity is normalized by concentration (data not shown). However, due to the reduced radius compared to the typical MCs, the SANS data for the low-T_{gel} material does not completely superpose with the other series after normalization; at low q they superpose, but the break in slope to $\approx q^{-4}$ behavior occurs at slightly higher q.

The SANS results clearly show that in the gel state the fibrillar structure is prevalent. The independence of the fibrillar structure with respect to M_w, spatial/regiochemical distribution of substituents, and concentration indicates that the tendency toward fibril formation is an intrinsic property of the polymer backbone. To explore this concept, SANS experiments were performed on dilute solutions well below the overlap concentration (c^*, calculated as the reciprocal of the intrinsic viscosity), so that the solutions have insufficient concentration to form gels. Figure 3 shows the SANS curves for three M_w and both types of MCs at 70 °C. The nature of the curves together with the model fits shows that even in the dilute regime, below c^*, MC chains adopt a fibrillar structure whose dimensions are very similar to those in the gel state (fibril diameter ≈ 13 nm). It is important to note, however, that at such low concentrations the MC fibrils are too few in number to percolate to form a gel.

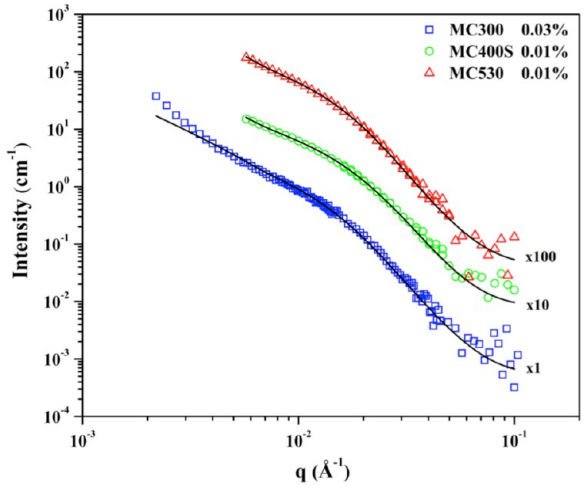

Figure 3. Scattering intensity versus scattering vector q at 70 °C for non-gelling MC solutions with low mass fractions. To aid in visualization, the traces have been vertically shifted by the factors indicated. Black lines are the best fits to eq 1, which have been shifted by the same factor as the respective data.

Internal Structure of Fibrils. SANS investigations for an extensive concentration series for MC300 were carried out, as shown in Figure 4 (points). The reproducibility of the scattering due the fibrillar structure is observed for samples that span well over an order of magnitude in concentration. Moreover, when the scattered intensity is normalized by concentration, all curves superpose onto a single trace (Figure S2). This indicates that the mesh size in the gels is larger than the range captured in the SANS experiments, and therefore modeling of data in the absence of a gel structure factor is valid.

The modeling of the SANS data allows for more nuanced information to be extracted from the results. An important consideration is the composition of the fibrils in the gel state; i.e., is there a solvent component to the fibrils? The treatment that follows provides a method to calculate the fibril composition, assuming that in the gel state all chains in the sample are incorporated into fibrils. This requires the selection of a temperature to be considered as the "fully developed" fibril state. We have selected 70 °C to be the temperature at which all chains are incorporated into fibrils. While this is somewhat arbitrary, there are several factors that support this selection. Using ^{1}H NMR spectroscopy to track methyl proton dynamics during the course of gelation, several groups have found the signal to disappear in the vicinity of 70 °C, indicating the immobilization of the protons.[4,38] In addition, this is the lowest temperature for which we have data, at which SANS traces superpose after normalization for concentration. It is also the temperature where the rheological properties and turbidity

dx.doi.org/10.1021/ma4021642 | Macromolecules 2013, 46, 9760−9771

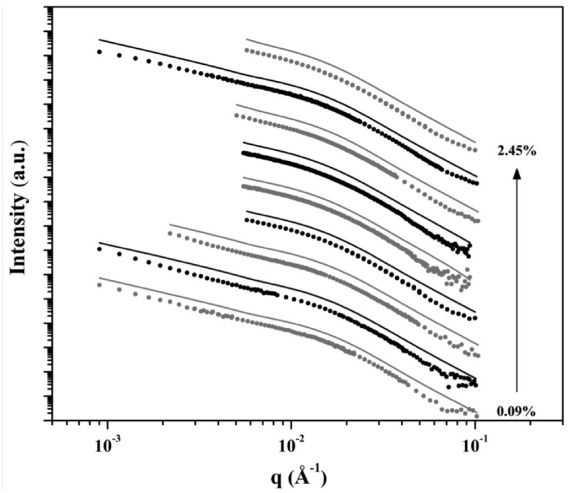

Figure 4. Scattering intensity versus scattering vector q at 70 °C (points) for MC300 gels. The traces have been arbitrarily shifted to aid visualization. Solid lines are predicted by eq 1 based on the scattering length density and volume fraction for fibrils that are 100% MC. Each model curve has been shifted the same amount as its corresponding data set.

begin to plateau. Thus, 70 °C is an appropriate temperature for a "fully developed" gel state.[58]

Equation 1 treats the fibrils as a collection of cylindrical objects, and the overall intensity scales as $\phi_{cy1}(\Delta\rho)^2$. If each cylinder contains only a fraction of polymer, x, then the effective volume of cylinders (ϕ_{cy1}) in eq 1 will be greater than the volume fraction of MC in the sample (ϕ_{MC}) according to

$$\phi_{MC} = \phi_{cy1}/x \tag{2}$$

due to the presence of solvent within the cylinder. The scattering length density (SLD) of the mixed-component cylinder (ρ_{cy1}) is equal to a volumetric average of the SLDs of MC (ρ_{MC}) and D_2O (ρ_{D_2O}) components, which are known:

$$\rho_{cy1} = x\rho_{MC} + (1 - x)\rho_{D_2O} \tag{3}$$

Therefore, the square of the contrast between the cylinder and surrounding solvent (D_2O) can be written as

$$(\rho_{cy1} - \rho_{D_2O})^2 = [(x\rho_{MC} + (1 - x)\rho_{D_2O}) - \rho_{D_2O}]^2 = x^2(\rho_{MC} - \rho_{D_2O})^2 \tag{4}$$

Combining eqs 2 and 4 results in the relationship

$$I(q) \sim x \tag{5}$$

Given that both the fraction of MC in the sample (ϕ_{MC}) and the SLD of MC (ρ_{MC}) are known, we can use eq 1 to predict what the scattering curve would be assuming the fibrils are 100% MC. These results are shown as the solid lines in Figure 4. To generate the curves, the data were first fit by varying ϕ_{cy1} and ρ_{MC} as well as the physical parameters of radius, dispersity in radii, and Kuhn length to match the intensity and shape, respectively, for the actual data. Next, all the parameters were held constant at the values for the best fit, and the variables ϕ_{cy1} and ρ_{cy1} were set to values corresponding to fibrils of 100% MC, i.e., $x = 1$, $\phi_{cy1} = \phi_{MC}$, and $\rho_{cy1} = \rho_{MC}$ to arrive at the $I(q)$ vs q curves displayed in Figure 4. It is apparent that across the entire concentration range this prediction yields intensities that are systematically higher than what is measured, indicating that there must be some solvent within the fibrils. The ratio of the predicted (solid) and measured (points) traces in Figure 4 (equal to x^{-1}) was taken for each sample at every data point in the q range of 0.005−0.07 Å^{-1}. The same treatment was applied to the SANS data for MC of different M_w (Figures S3a−S3d). Thus, the average composition of the fibrils in the gel state at 70 °C was found to be 40 ± 5% and 49 ± 8% for the typical and low-T_{gel} MCs, respectively.

Figure 5 contains the results for the fibril radius, volume fraction of fibril that is MC, and Kuhn length of the fibrils

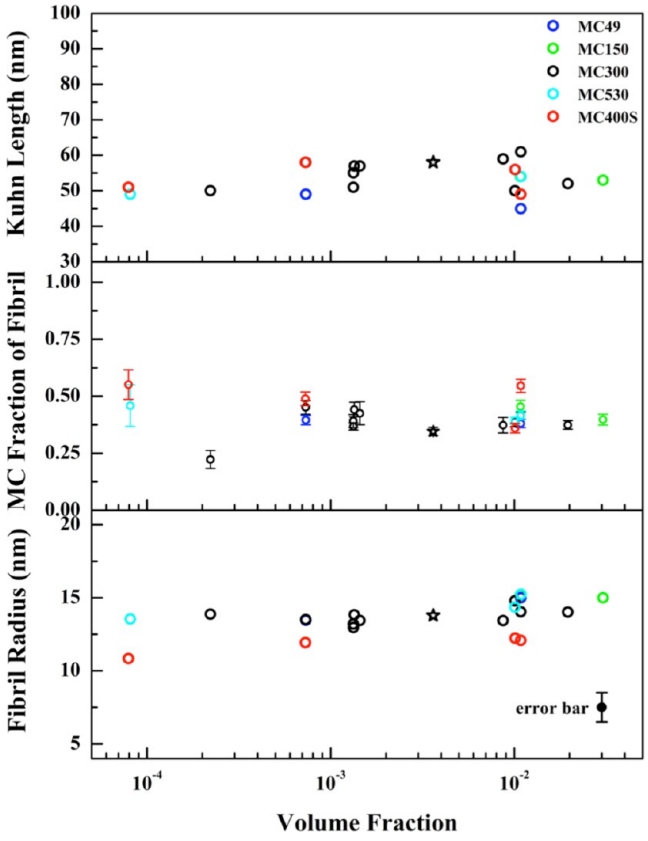

Figure 5. Fibril radius (lower panel), volume fraction of MC within a fibril (middle panel), and fibril Kuhn length (upper panel) for MC49 (blue), MC150 (green), MC300 (black), MC530 (cyan), and MC400S (red) at 70 °C. The stars represent experiments conducted at 65 °C.

obtained from the modeling. The values are essentially constant over all the samples studied. This corroborates both cryo-TEM and SANS findings that suggest that the fibrillar structure is independent of M_w and concentration.

Solution State. Both cryo-TEM and SANS taken at low temperatures (solution state) show no trace of fibrillar structures.[1] Figure 6 shows typical SANS data for semidilute solutions of MC with different M_w. The shoulder at $q \approx 0.015$ Å^{-1} observed for MC gels is not present in the scattering profile for the solutions. The nature of these curves at low q obeys the power-law behavior previously noted by Chatterjee et al.[38] They employed an empirical model to fit their data:

$$I(q) = aq^{-m} + \frac{I(0)}{1 + q^2\xi^2} + BD \tag{6}$$

where the aq^{-m} term captures the power-law behavior at low q. The Ornstein−Zernike relation describes the behavior at higher

dx.doi.org/10.1021/ma4021642 | Macromolecules 2013, 46, 9760−9771

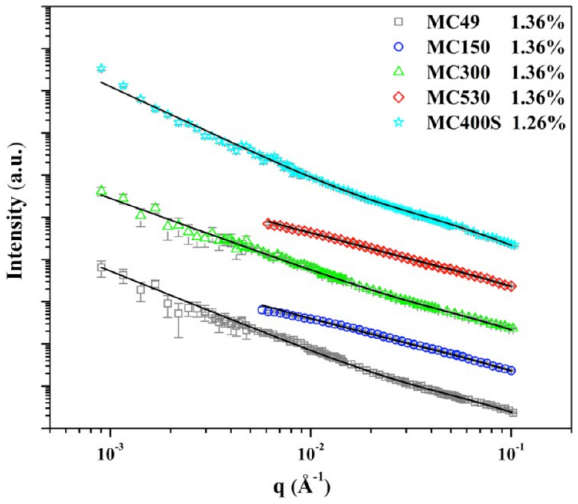

Figure 6. Scattering intensity versus scattering vector q for MC solutions at 25 °C (cyan) and 30 °C (gray, blue, green, red) for similar mass fractions. To aid in visualization, the traces have been vertically shifted. Black lines are the best fits to eq 6, which have been shifted by the same factor as the respective data.

q in terms of the zero-scattering-vector structure factor ($I(0)$) and the polymer concentration fluctuation length (ξ), along with a term for background (BD). We have successfully applied eq 6 to fit our solution-state SANS data as shown by the black lines in Figure 6. The low-q power-law slopes had an average value of 2.6 that did not depend on M_w or concentration. For the purposes of our current study, we are not primarily concerned with the exact values obtained for the fitting parameters (Table S2). However, we will employ this model as a baseline as we probe the scattering recorded throughout the sol−gel transition.

Transformation of Chains to Fibrils. So far we have examined the two limits of the temperature range where the scattering is well-defined; high temperatures give rise to scattering from the fibrillar network, and low temperature scattering is a result of the semidilute polymer solution. However, the intermediate temperature range over which the sol−gel transition occurs is also of interest as that is where the fibrillar structure forms. As the temperature is increased, SANS curves increase in intensity and the shoulder at $q \approx 0.015$ Å^{-1} develops. Previous cryo-TEM results showed that at pregel temperatures (55 °C) a very small amount of fibrils form that have the same diameter of ≈15 nm.[1] With this in mind, we hypothesize that the scattering at such temperatures should not reflect the growth of fibrils with different physical dimensions, but rather be the result of a combination of two components: fibrils with the same composition and dimension as found at 70 °C and free chains with the same characteristics as found at low temperatures (25−30 °C). We therefore use linear combinations of the solution and gel-state scattering functions to fit the data at intermediate temperatures to arrive at the relative fractions of the polymer in each state. Thus, we are able to track the full progression of fibril growth with temperature for aqueous MC materials.

Figure 7a contains SANS data (open points) recorded at various temperatures for an MC300 sample with a mass fraction of 1.36%. The solid lines represent the best fits to the data; the highest temperature trace was fit using eq 1, the lowest temperature trace was fit using eq 6, and the intermediate temperatures were fit using linear combinations thereof. At higher q there is some minor discrepancy between the data and the fits partly due to the fact that a single background term, extracted from the high temperature data using eq 1, is used for all temperatures. The balance between solution and gel scattering required to approximate the scattering data at intermediate temperatures gives the fraction of polymer of the sample that has been incorporated into the fibril state at a given temperature. Figure 7b contains a plot of the results of this treatment for several concentrations of MC300. It is important to note that due to the nucleation and growth-type development of the MC gel structure, the thermal histories of the various experiments are important and not always well matched, and therefore detailed comparison should be avoided. Rather, the graph is provided to illustrate that at low temperatures there is no trace of fibrils; since the gel structure scatters much more intensely than the solution state, the presence of ≤1% of fibrils is readily detectable. In addition, as we have set 70 °C to be a temperature at which 100% of the chains are incorporated into fibrils, the mole fraction of MC in the fibrils plateaus at unity once 70 °C is reached. The temperature regime for the growth of fibrils corresponds to what we have observed in cryo-TEM experiments and is consistent with the temperatures at which gelation and clouding occur. Figure 7c shows the aforementioned treatment applied to MC with varying M_w and shows the same trends as Figure 7b. In addition, the same independence on M_w for fibril growth is seen, as previously reported for T_{gel}.[40]

Hysteresis during Cooling. SANS and cryo-TEM clearly relate the growth of fibrils with the macroscopic properties of rheology and turbidity during heating. Hysteresis upon cooling has been widely observed in MC gels because the structure developed during gelation persists until the sample is sufficiently cooled, as directly captured by optical micrographs of samples during heating and cooling.[39] If the ultimate MC gel structure is in fact fibrillar, nanoscale micrographs should reveal the presence of fibrils during the cooling cycle. Figure 8 contains cryo-TEM images taken for a sample that was only heated to 50 °C and for one that was first heated to 70 °C for 30 min and then annealed at 50 °C for 30 min. This temperature was chosen because previous cryo-TEM experiments found no occurrence of fibrils during heating, and rheological experiments show the hysteresis is prevalent at this temperature during cooling. The fibrillar structure is clearly observed in Figure 8b and confirms that the hysteresis in rheology results from the continued presence of the network structure even during cooling.

SANS experiments were used to confirm and quantify the qualitative microscopy results. Figure 9 contains SANS curves for the MC300 material in D_2O as it was heated and subsequently cooled over the range of 25−75 °C. The hysteresis observed in rheological traces is also apparent in the SANS data. Particularly noteworthy is that during cooling the relative change in intensity is small until a temperature of ≈40 °C is reached. As the sample is further cooled, the intensity rapidly drops off, particularly once the sample is cooled to 30 °C. This is in excellent agreement with previous findings in rheological[39,40] and DSC[4,58,59] experiments in which the gel dissolution temperature was found to consistently be in the vicinity of 30 °C independent of the cooling rate used.

The analysis using linear combinations of hot gel and solution scattering curves can be applied to the data in Figure 9 to track both the formation and dissolution of the fibrillar structure as the material is heated and cooled. The results of

dx.doi.org/10.1021/ma4021642 | Macromolecules 2013, 46, 9760−9771

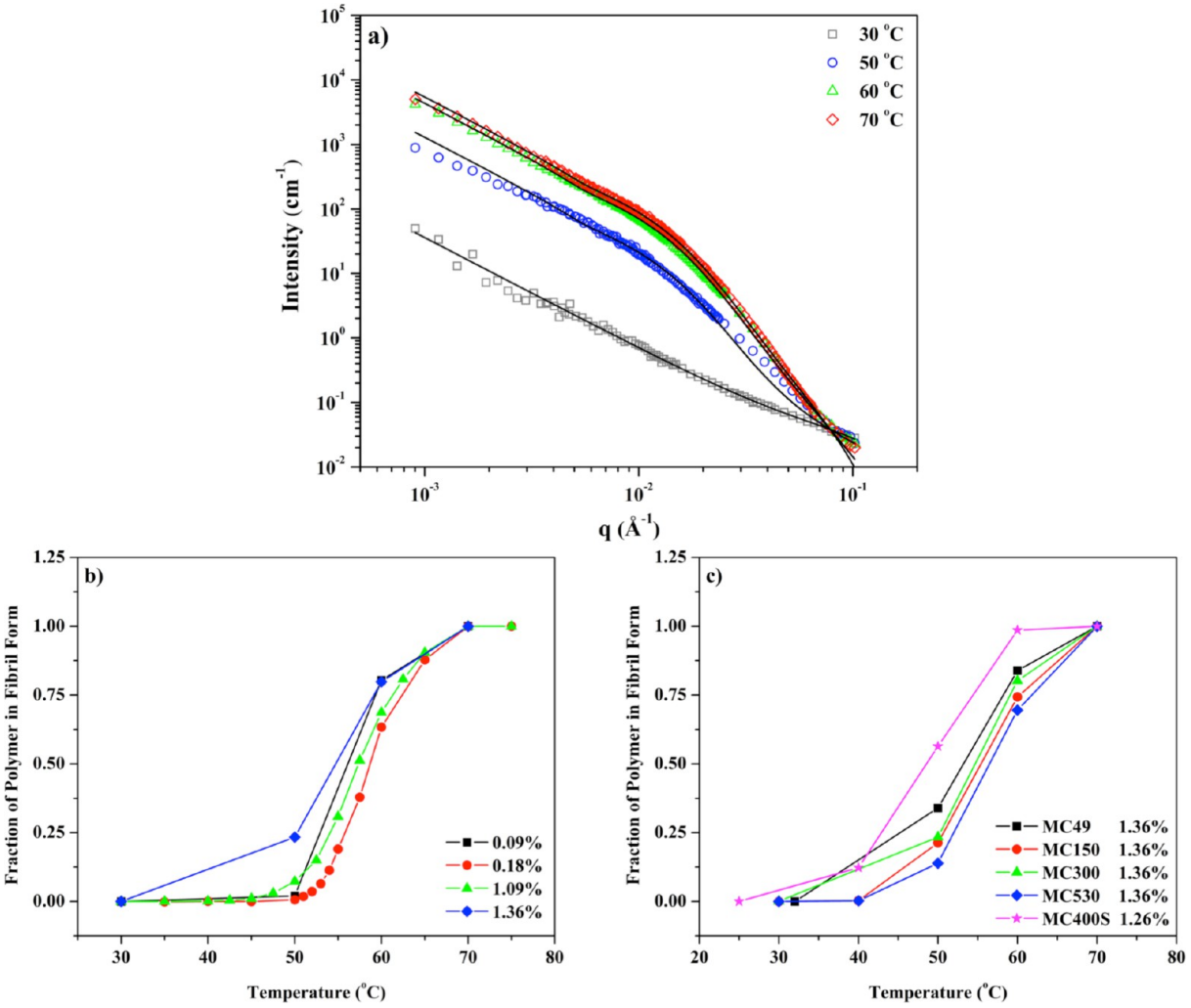

Figure 7. (a) Scattering intensity versus scattering vector q (open points) at selected temperatures for an MC300 solution with a mass fraction of 1.36%. The black lines are the fit to eq 6 (32 °C) and eq 1 (70 °C) and linear combinations thereof (50 and 60 °C). (b) Calculated fraction of total MC incorporated into fibrils for MC300 at various concentrations. (c) Calculated fraction of total MC incorporated into fibrils for MC of varying M_w.

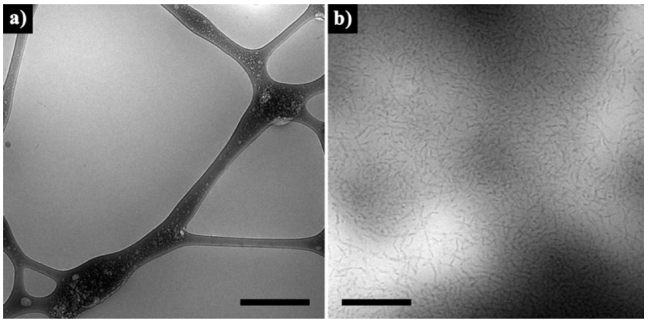

Figure 8. Cryo-TEM images of MC300 solutions with a mass fraction of 0.20%: (a) annealed for 30 min at 50 °C and then rapidly vitrified (with the lacey carbon support grid visible); (b) annealed for 30 min at 70 °C followed by 30 min 50 °C and then rapidly vitrified. Scales bars represent 500 nm.

this analysis are presented in Figure 10. The results from the SANS experiments bear a remarkable resemblance to the rheological properties. To further corroborate the relationship between fibril formation and rheological properties, a series of frequency sweeps were performed on an aqueous MC300 sample with a mass fraction of 1.09% in such a way as to match the thermal history of the SANS experiments. As shown in Figure 10, the agreement between the two experiments confirms that the gelation behavior for MC is a direct result of the fibrillar network structure.

Ultrasmall-Angle Neutron Scattering (USANS). To expand the scope of scattering experiments, we utilized USANS[60] measurements to examine larger-scale features of the MC gels. Desmeared USANS data collected at 50 and then 70 °C for a several MC samples are shown along with the corresponding SANS curves in Figure 11. The overlap in the scattering curves from the two techniques is very good, validating the USANS desmearing algorithm in addition to the absolute scaling of both sets of data. The combination of SANS and USANS provides a depiction of MC scattering over a broader q range. The USANS data captures the same $q^{-1.7}$ behavior as observed in the SANS experiments. At 70 °C, the gel samples display an upturn in slope that is thought to correlate with the heterogeneity in the fibril network density observed in cryo-TEM experiments that accounts for the turbidity of MC gels. It is interesting to note that the q value at which the slope changes seems to correlate with M_w, indicated

dx.doi.org/10.1021/ma4021642 | Macromolecules 2013, 46, 9760−9771

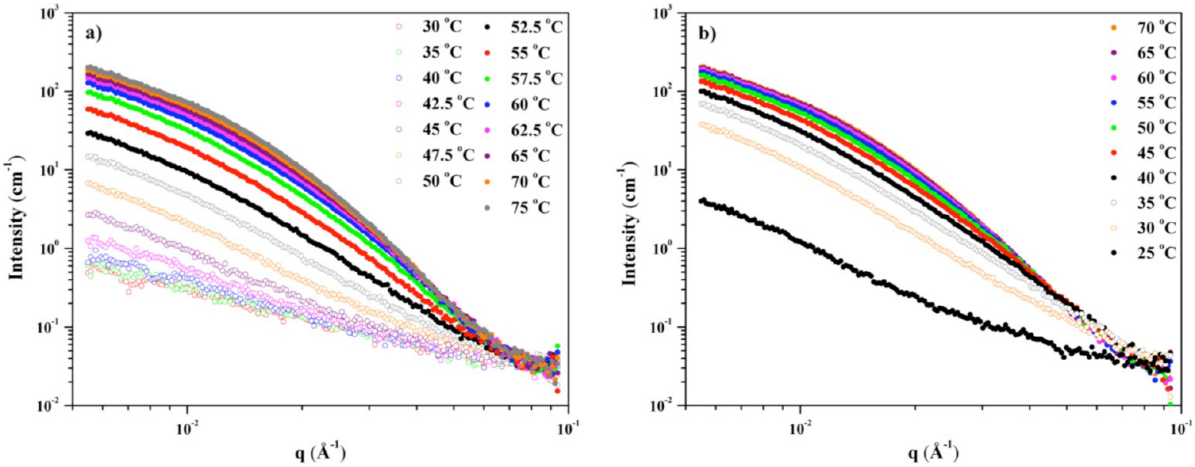

Figure 9. Scattering intensity versus scattering vector q at selected temperatures for a MC300 solution with a mass fraction of 1.09% during (a) heating and (b) cooling.

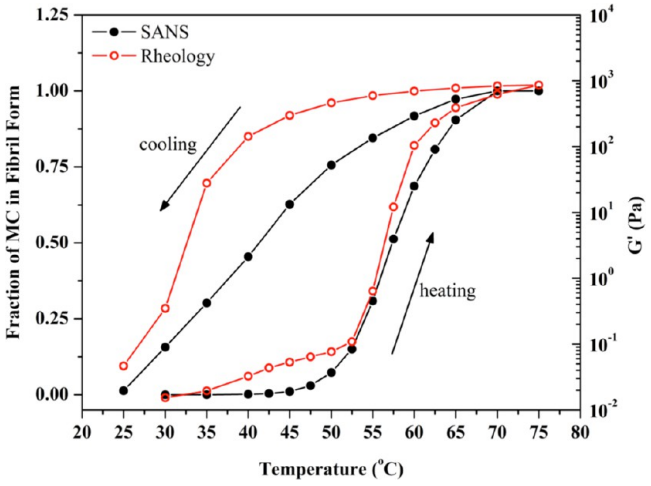

Figure 10. Fraction of the total polymer chains that are incorporated into fibrils (filled, black points) as calculated by taking linear combinations of the solution (30 °C) and gel (70 °C) SANS curves for a MC300 solution with a mass fraction of 1.09%. Storage modulus (open, red points) for a MC300 sample with a mass fraction of 1.09% measured using a thermal history to match the SANS experiment. Values are for a frequency of 1 rad/s and 5% strain. In both traces, the connecting lines are provided as visual aids only and do not represent actual data.

with arrows in Figure 11. The lowest M_w investigated displays an upturn around ≈0.002 Å^{-1} (Figure 11c) that shifts to approximately 0.0003 Å^{-1} and 0.0001 Å^{-1} as M_w increases to 300 and 400 kg/mol, respectively (Figures 11a,b,e). For the largest M_w sample, the upturn appears to be shifted out of the q range; however, at the lowest q a beginning of an upturn may be present (Figure 11d). The corresponding size scales of these features are on the order of ≈1−5 μm. Features of comparable size have been reported from FFT of optical micrographs (5 μm)[39] as well as light scattering (1.5 μm)[61] of aqueous MC. The fact that no plateau region is present at the lowest q range indicates that heterogeneities persist beyond the largest length scale accessed (≈20 μm). The upturns in the USANS data adopt a $I(q) \approx q^{-3.5}$ dependence, which approaches Porod behavior. This may indicate that MC fibrils aggregate into micron-sized "fibril-rich" and "fibril-poor" regions, and the Porod-like scattering reflects the interfaces between the two.

DISCUSSION

The analysis of scattering data for MC solutions and gels has typically employed the use of generalized scattering functions[36−38,61] of the Ornstein−Zernike or Debye−Bueche type, or modified versions thereof, such as the Bastide equation[62] for scattering from polymer gels. In SAXS experiments, Takahashi et al. examined MC solutions with a mass fraction of 0.9% as they were heated from the solution state into the gel state.[37] To analyze the scattering data, a Guinier term was used to calculate a characteristic length (R_G), which increased sharply around the sol−gel transition and was 2.3, 5.7, and 6.4 nm at 50, 60, and 65 °C, respectively. In the high temperature gel regime, R_G changed less with temperature, increasing from 6.4 to only ≈7 nm from 65 to 80 °C.

Kobayashi and co-workers employed SANS to probe the structure of MC gels.[36] To model the data over the entire q range measured, a Debye−Bueche term was added to the Bastide scattering function along with a cutoff factor as described by Coviello et al.[63] This treatment resulted in the extraction of two length scales: a larger scale feature of 120 nm, interpreted as the correlation length of the gel network, and a short-range structural element of 5.4 nm referred to as the radius of the cross-linking zones. A similar approach was recently reported by Chatterjee et al. on MC gels,[38] who found a gel correlation length of ≈110 nm and a smaller-scale feature of ≈7.5 nm. In these SANS studies, the larger feature of 110−120 nm implies a plateau in the scattering intensity that lies outside the measured q range. Features of these dimensions fail to explain the opacity of the gels at elevated temperatures. Also, the correlation length was found to be independent of concentration, which contradicts a "blob-like" depiction of these gels where the mesh size should vary strongly with concentration. We note that in the aforementioned reports the size of the smaller feature corresponds nicely to the radius of the fibrils.

Our treatment of the growth of fibrils during the sol−gel transition is based on the assumption that at 70 °C all the chains in the sample are incorporated into fibrils. However, for SANS measurements conducted at temperatures above 70 °C (Figure S5), MC samples display increased scattering as the temperature is raised from 70 to 90 °C. The increase in overall SANS intensity across this temperature range is approximately 25 and 10% for standard and low-T_{gel} materials, respectively.

dx.doi.org/10.1021/ma4021642 | Macromolecules 2013, 46, 9760−9771

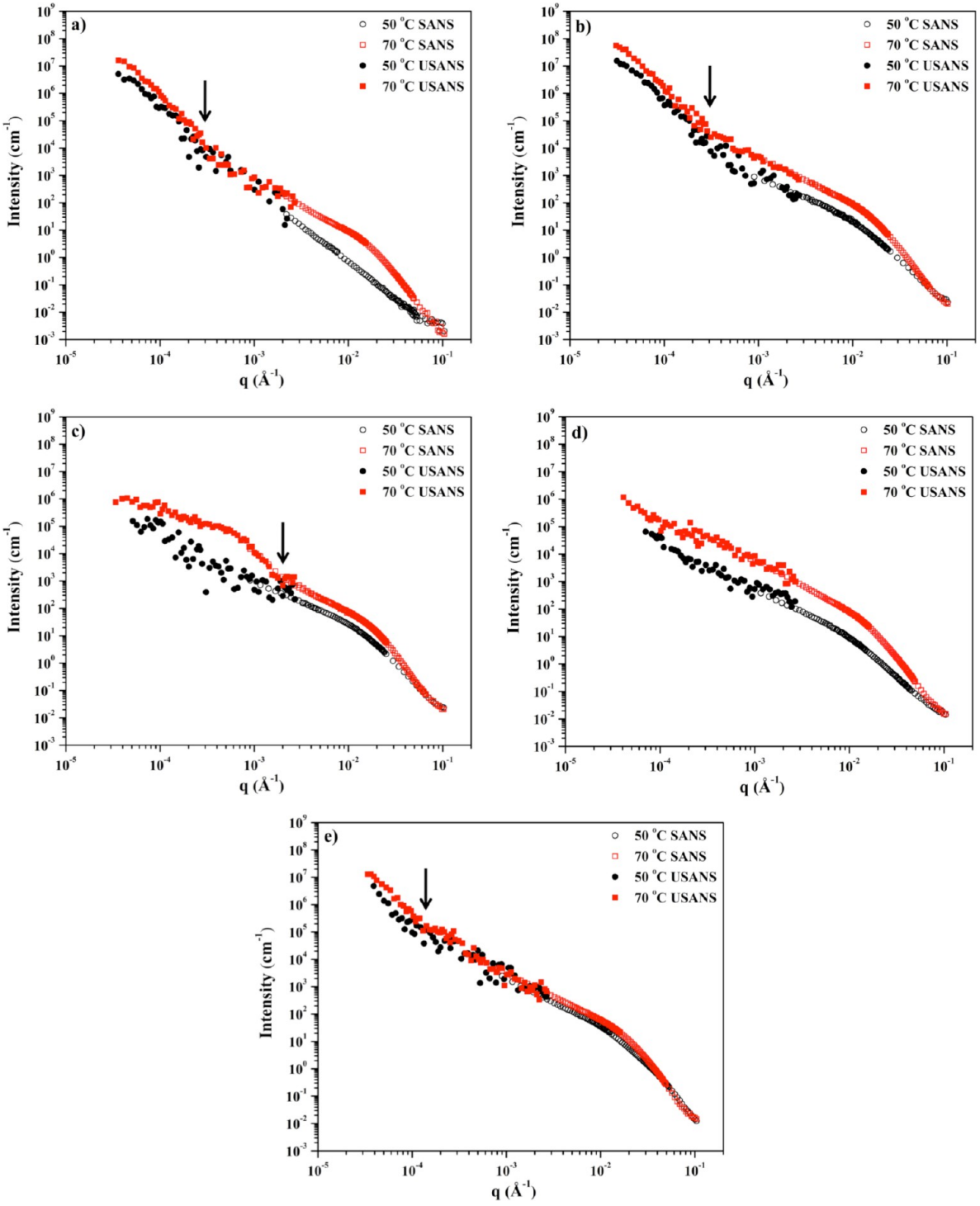

Figure 11. USANS (solid) and SANS (open) data collected at 50 °C (black, circles) and 70 °C (red, squares) for MC samples with mass fractions of (a) 0.17% MC300, (b) 1.26% MC300, (c) 1.36% MC49, (d) 1.26% MC530, and (e) 1.26% MC400S.

This change is much smaller than the increase of orders of magnitude recorded in the vicinity of T_{gel}. In addition, fitting the 80 and 90 °C data with eq 1 (Table S1) reveals that the fibril radii do not change as the sample is heated above 70 °C. We propose that the most likely scenario is that the fibrils expel solvent at elevated temperatures. This is consistent with many reported observations of syneresis from MC gels at elevated temperatures.[3,38,64,65] Expulsion of D_2O from the fibrils decreases the effective scattering length density of the fibril as well as the volume fraction of the fibrils. Since $I \sim \phi_{cyl}(\Delta\rho)^2$, the decrease in fibril volume fraction causes a decrease to scattering intensity; however, this is overshadowed by the corresponding increase in $\Delta\rho$, and a net increase to scattering intensity is observed. Increasing temperature from 70 to 90 °C corresponds to a change in the fibril composition from ≈40 to 50% MC. For the low-T_{gel} material, the corresponding change is from 50 to 60% as the sample is heated from 70 to 90 °C.

An alternative scenario is that there remains a portion of chains that have not taken part in the fibrillar network at 70 °C. In this situation, an increasing fraction of chains become

dx.doi.org/10.1021/ma4021642 | Macromolecules 2013, 46, 9760−9771

incorporated into fibrils as the temperature is increased from 70 to 90 °C. If 90 °C is taken as a point at which 100% of the chains are incorporated in fibrils, then at 70 °C roughly 15% of the chains remain in a nonfibril state.

The finding that water occupies a significant portion of the fibrils indicates there may be different modes of binding between the water within the interior of the fibril and the water that makes up the vast (>95%) majority of the gel. Indeed, as MC is hygroscopic in nature, several groups have studied hydration and swelling properties as well the binding of water to MC powders, films, and gels.[66−72] Because of the heterogeneous substitution of the MC chains, many types of water−polymer interactions are possible. Fourier transform infrared (FT-IR) spectroscopy measurements can monitor the growth and/or perturbation of characteristic absorption peaks that can be assigned to specific molecular interactions such as those involving hydroxyl groups. FT-IR experiments have revealed a number of water−water and water−polymer interactions, among them water−polymer hydrogen bonds. In a simple approximation, the binding state of a particular water molecule to the MC chain can be described by one of two states: free and tightly bound. DSC measurements can determine the amount of free water by measuring the portion of the water in the sample that is able to freeze at low temperatures. Water that is tightly bound to the polymer chain lacks the mobility required to freeze, so the population that is tightly bound will not contribute to the thermal event recorded in DSC thermograms. Using this approach, several groups have calculated the stoichiometry of the fully hydrated solution state and found that there are 5−6 mol of water bound per mole MC repeat unit.[67,72] If one disregards the free water in the solution and considers a system containing only the tightly bound water molecules and the polymer chains, the resulting volume fraction of MC would be ≈60%. The SANS data presented here give no indication as to whether solvent within the fibrils is "bound" to MC or not. However, given the large excess of water in the gels (>95% solvent), it is interesting to note that the ratio of tightly bound water to polymer at low temperatures is similar to the ratio of solvent to polymer within each fibril, at high temperatures in the gel state. The internal structure of the fibrils poses a very interesting question that is currently under investigation.

SUMMARY

For MC (DS = 1.8) with 49 < M_w < 530 kg/mol and mass fractions of 0.01 < c < 3.79%, the fibrillar gel structure was found to be dominant at elevated temperatures. At low temperatures (≤30 °C) no fibrils were detected. The dimensions of the fibrils were independent of the polymer M_w, spatial/regiochemical distribution of methoxy moieties, or concentration. The fibrils have diameters and Kuhn lengths of roughly 15 and 50 nm, respectively. The presence of the fibrils in aqueous MC samples that had been cooled from elevated temperatures to 50 °C confirms that the rheological hysteresis observed is a result of the fibril structure. It was found that the fibrils contain a significant portion of water and that MC occupies about 40% of the total volume of the fibril.

APPENDIX

The overall scattering function used to model the fibrils is

$$I_{WC}(q, L, b, R_{CS}) = \phi_{cyl}(\Delta\rho)^2 S_{WC}(q, L, b) P_{CS}(q, R_{CS}) + BD \tag{A.1}$$

where q is the scattering wave vector, L is the contour length of the fibril, b is the Kuhn length of the fibril, R_{CS} is the radius of the cross section of the fibril, ϕ_{cyl} is the volume fraction of fibrils, $\Delta\rho$ is the contrast in scattering length density between the fibrils and the solvent, and BD is a background correction term.

$P_{CS}(q,R_{CS})$ is the scattering function for the cross section of a rigid rod and defined as

$$P_{CS}(q, R_{CS}) = \left[\frac{2J_1(qR_{CS})}{qR_{CS}}\right]^2 \tag{A.2}$$

where $J_1(x)$ is the Bessel function of the first kind.

$S_{WC}(q,L,b)$ is the scattering function for semiflexible chains with excluded volume effects.

For qb < 3.1:

$$S_{WC}(q, L, b) = S_{exv}(q, L, b) + \frac{C(n_b)}{n_b}\left[\frac{4}{15} + \frac{7}{15u} - \left(\frac{11}{15} + \frac{7}{15u}\right)\exp(-u)\right] \tag{A.3}$$

$$S_{exv}(q, L, b) = [1 - w(qR_g)]S_{Debye}(q, L, b) + f(q)w(qR_g)[1.22(qR_g)^{-1/0.585} + 0.4288(qR_g)^{-2/0.585} - 1.651(qR_g)^{-3/0.585}] \tag{A.4}$$

where $f(q)$ is defined as

$$f(q) \equiv \begin{cases} 1 & \text{for } \dfrac{dS(q, L, b)}{dq} \le 0 \\ 0 & \text{for } \dfrac{dS(q, L, b)}{dq} > 0 \end{cases} \tag{A.5}$$

$$S_{Debye}(q, L, b) = 2[\exp(-u) + u - 1]/u^2 \tag{A.6}$$

$$u = \frac{Lb}{6}\left\{1 - \frac{3}{2n_b} + \frac{3}{2n_b^2} - \frac{3}{4n_b^3}[1 - \exp(-2n_b)]\right\}q^2 \tag{A.7}$$

$$n_b = \frac{L}{b} \tag{A.8}$$

$$w(x) = \frac{1 + \tanh[(x - 1.523)/0.1477]}{2} \tag{A.9}$$

$$\langle R_g^2\rangle = \alpha(n_b)^2 bL/6 \tag{A.10}$$

$$\alpha(x) = \sqrt{[1 + (x/3.12)^2 + (x/8.67)^3]^{0.176/3}} \tag{A.11}$$

$$C(n_b) = \begin{cases} 3.06n_b^{-0.44} & \text{for } L > 10b \\ 1 & \text{for } L \le 10b \end{cases} \tag{A.12}$$

For $qb \ge 3.1$:

$$S_{WC} = \frac{a_1(q, L, b)}{(qb)^{4.95}} + \frac{a_2(q, L, b)}{(qb)^{5.29}} + \frac{\pi}{qL} \tag{A.13}$$

The expressions for $a_1(q,L,b)$ and $a_2(q,L,b)$ are provided in ref 45.

dx.doi.org/10.1021/ma4021642 | Macromolecules 2013, 46, 9760−9771

■ ASSOCIATED CONTENT

Supporting Information

Figures S1−S5; Tables S1 and S2. This material is available free of charge via the Internet at http://pubs.acs.org.

■ AUTHOR INFORMATION

Corresponding Authors

*E-mail: bates001@umn.edu (F.S.B.).
*E-mail lodge@umn.edu (T.P.L.).

Notes

The authors declare no competing financial interest.

■ ACKNOWLEDGMENTS

The authors thank Paul Butler, Steven Kline, Yun Liu, Lilin He, and Yuri Melnichenko for valuable dialogue concerning SANS and Robert Hafner for his helpful guidance concerning cryo-TEM experiments. Discussions with Robert Schmitt, Meinolf Brackhagen, and Tirtha Chatterjee were very helpful. This work was funded by a business unit (Dow Pharma and Food Solutions) of The Dow Chemical Company. Cryo-TEM measurements were carried out in the CSE Characterization Facility, University of Minnesota, which receives partial support from NSF through the MRSEC program. We acknowledge the support of the National Institute of Standards and Technology, which utilized facilities supported in part by the National Science Foundation under Agreement DMR-0944772, U.S. Department of Commerce, in providing the neutron research facilities used in this work. Part of the research conducted at ORNL's High Flux Isotope Reactor was sponsored by the Scientific User Facilities Division, Office of Basic Energy Sciences, U.S. Department of Energy. Certain commercial equipment, instruments, or materials are identified in this paper to foster understanding. Such identification does not imply recommendation or endorsement by the National Institute of Standards and Technology, nor does it imply that the materials or equipment identified are necessarily the best available for the purpose.

■ REFERENCES

(1) Lott, J. R.; McAllister, J. W.; Arvidson, S. A.; Bates, F. S.; Lodge, T. P. *Biomacromolecules* **2013**, *14*, 2484.
(2) Denham, W. S.; Woodhouse, H. *J. Chem. Soc., Faraday Trans.* **1913**, *103*, 1735.
(3) Heymann, E. T. *Faraday Soc.* **1935**, *31*, 846.
(4) Haque, A.; Morris, E. R. *Carbohydr. Polym.* **1993**, *22*, 161.
(5) Guillot, S.; Lairez, D.; Axelos, M. A. V. *J. Appl. Crystallogr.* **2000**, *33*, 669.
(6) Bodvik, R.; Dedinaite, A.; Karlson, L.; Bergstrom, M.; Baverback, P.; Pedersen, J. S.; Edwards, K.; Karlsson, G.; Varga, I.; Claesson, P. M. *Colloids Surf., A* **2010**, *354*, 162.
(7) Bodvik, R.; Karlson, L.; Edwards, K.; Eriksson, J.; Thormann, E.; Claesson, P. M. *Langmuir* **2012**, *28*, 13562.
(8) Klemm, D.; Heublein, B.; Fink, H.-P.; Bohn, A. *Angew. Chem., Int. Ed.* **2005**, *44*, 3558.
(9) *Molecular Gels Materials with Self-Assembled Fibrillar Networks*; Weiss, R. G., Terech, P., Eds.; Springer: Dordrecht, The Netherlands, 2006.
(10) Greer, S. C. *Annu. Rev. Phys. Chem.* **2002**, *53*, 173.
(11) Tuszynski, J. A.; Brown, J. A.; Sept, D. J. *Biol. Phys.* **2003**, *29*, 401.
(12) Oakley, B. R.; Akkari, Y. N. *Cell Struct. Funct.* **1999**, *24*, 365.
(13) Fuchs, E. *Ann. Rev. Cell Dev. Biol.* **1995**, *11*, 123.
(14) Smack, D. P.; Korge, B. P.; James, W. D. *J. Am. Acad. Dermatol.* **1994**, *30*, 85.
(15) Caria, A.; Bixio, L.; Kostyuk, O.; Ruggerio, C. *IEEE Trans. Nanobiosci.* **2004**, *3*, 85.
(16) Wallace, D. G.; Rosenblatt, J. *Adv. Drug Delivery Rev.* **2003**, *55*, 1631.
(17) Suguyama, J.; Rochas, C.; Turquois, T.; Taravel, F.; Chanzy, H. *Carbohydr. Polym.* **1994**, *23*, 261.
(18) Yang, Y. C.; Geil, P. H. *J. Macromol. Sci., Phys. B* **1983**, *3*, 463.
(19) McKenna, G. B.; Guenet, J. M. *J. Polym. Sci., Polym. Phys. Ed.* **1988**, *26*, 267.
(20) Fazel, Z.; Fazel, N.; Guenet, J. M. *J. Phys. II* **1992**, *2*, 1745.
(21) Cornelissen, J. J. L. M.; Fischer, M.; Sommerdijk, N. A. J. M.; Nolte, R. J. M. *Science* **1998**, *280*, 1427.
(22) Newbloom, G. M.; Weigandt, K. M.; Pozzo, D. C. *Soft Matter.* **2012**, *8*, 8854.
(23) Praveen, V. K.; George, S. J.; Ajayaghosh, A. *Macromol. Symp.* **2006**, *241*, 45.
(24) Rammensee, S. P.; Janmey, P. A.; Bausch, A. R. *Eur. Biophys. J.* **2007**, *26*, 661.
(25) Shah, J. V.; Janmey, P. A. *Rheol. Acta* **1997**, *36*, 262.
(26) Petkova, A. T.; Ishii, Y.; Balbach, J. J.; Antzutkin, O. N.; Leapman, R. D.; Delaglio, F.; Tycko, R. *Proc. Natl. Acad. Sci. U. S. A.* **2002**, *99*, 16742.
(27) MacKintosh, F. C.; Käs, J.; Janmey, P. A. *Phys. Rev. Lett.* **1995**, *75*, 4425.
(28) Gardel, M. L.; Shin, J. H.; MacKintosh, F. C.; Mahadevan, L.; Matsudaira, P.; Weitz, D. A. *Science* **2004**, *304*, 1301.
(29) Storm, C.; Pastore, J. J.; MacKintosh, F. C.; Lubensky, T. C.; Janmey, P. A. *Nature* **2005**, *435*, 191.
(30) Bausch, A. R.; Kroy, K. *Nat. Phys.* **2006**, *2*, 231.
(31) Janmey, P. A.; McCormick, M. E.; Rammensee, S.; Leight, J. L.; Georges, P. C.; MacKintosh, F. C. *Nat. Mater.* **2007**, *6*, 48.
(32) Lin, Y.-C.; Koenderink, G. H.; MacKintosh, F. C.; Weitz, D. A. *Macromolecules* **2007**, *40*, 7714.
(33) Van Dillen, T.; Onck, P. R.; Van der Giessen, E. *J. Mech. Phys. Solids* **2008**, *56*, 2240.
(34) Broedersz, C. P.; Kasza, K. E.; Jawerth, L. M.; Münster, S.; Weitz, D. A.; MacKintosh, F. C. *Soft Matter* **2010**, *6*, 4120.
(35) Žagar, G.; Onck, P. R.; Van der Giessen, E. *Macromolecules* **2011**, *44*, 7026.
(36) Kobayashi, K.; Huang, C.; Lodge, T. P. *Macromolecules* **1999**, *32*, 7070.
(37) Takahashi, M.; Shimazaki, M.; Yamamoto, J. *J. Polym. Sci., Polym. Phys.* **2000**, *39*, 91.
(38) Chatterjee, T.; Nakatani, A. I.; Adden, R.; Brackhagen, M.; Redwine, D.; Shen, H.; Li, Y.; Wilson, T.; Sammler, R. L. *Biomacromolecules* **2012**, *13*, 3355.
(39) Fairclough, J. P. A.; Yu, H.; Kelly, O.; Ryan, A. J.; Sammler, R. L.; Radler, M. *Langmuir* **2012**, *28*, 10551.
(40) Arvidson, S. A.; Lott, J. R.; McAllister, J. W.; Zhang, J.; Bates, F. S.; Lodge, T. P.; Sammler, R. L.; Li, Y.; Brackhagen, M. *Macromolecules* **2013**, *46*, 300.
(41) Reibert, K. C.; Conklin, J. R. Cellulose Ether Having Enhanced Gel Strength and Composition Containing It. US Patent US6228416 B1, 2001.
(42) Kline, S. R. *J. Appl. Crystallogr.* **2006**, *39*, 895.
(43) Pedersen, J. S.; Schurtenberger, P. *Macromolecules* **1996**, *29*, 7602.
(44) Jerke, G.; Pedersen, J. S.; Egelhaaf, S. U.; Schurtenberger, P. *Phys. Rev. E* **1997**, *56*, 5772.
(45) Chen, W.; Butler, P. D.; Magid, L. J. *Langmuir* **2006**, *22*, 6539.
(46) Glatter, O. *J. Appl. Crystallogr.* **1977**, *10*, 415.
(47) Kratky, O.; Porod, G. *Recl. Trav. Chim. Pays-Bas* **1949**, *68*, 1105.
(48) Takahashi, S.-I.; Fujimoto, T.; Miyamoto, T. *J. Polym. Sci., Polym. Chem.* **1987**, *25*, 987.
(49) Arisz, P.; Kauw, H. J. J.; Boon, J. J. *Carbohydr. Res.* **1995**, *271*, 1.
(50) Desbrières, J.; Hirrien, M.; Rinaudo, M. *Carbohydr. Polym.* **1998**, *37*, 145.
(51) Hirrien, M.; Chevillard, C.; Desbrières, J.; Axelos, M. A. V.; Rinaudo, M. *Polymer* **1998**, *39*, 6251.

(52) Itagaki, H.; Tokai, M.; Kondo, T. *Polymer* **1997**, *38*, 4201.
(53) Liu, H.; Zhang, L.; Takaragi, A.; Miyamoto, T. *Polym. Bull.* **1998**, *40*, 741.
(54) Kern, H.; Choi, S. W.; Wenz, G.; Heinrich, J.; Ehrhardt, L.; Mischnick, P.; Garidel, P.; Blume, A. *Carbohydr. Res.* **2000**, *326*, 67.
(55) Sekiguchi, Y.; Sawatari, C.; Kondo, T. *Carbohydr. Polym.* **2003**, *53*, 145.
(56) Parfondry, A.; Perlin, A. S. *Carbohydr. Res.* **1977**, *57*, 39.
(57) Erler, U.; Mischnick, P.; Klemm, D. *Polym. Bull.* **1992**, *29*, 349.
(58) Li, L. *Macromolecules* **2002**, *35*, 5990.
(59) Li, L.; Shan, H.; Yue, C. Y.; Lam, Y. C.; Tam, K. C.; Hu, X. *Lamgmuir* **2002**, *18*, 7291.
(60) Barker, J. G.; Glinka, C. J.; Moyer, J. J.; Kim, M. H.; Drews, A. R.; Agamalian, M. *J. Appl. Crystallogr.* **2005**, *38*, 1004.
(61) Takeshita, H.; Saito, K.; Miya, M.; Takenaka, K.; Shiomi, T. *J. Polym. Sci., Polym. Phys.* **2010**, *48*, 168.
(62) Bastide, J.; Leibler, L.; Prost, J. *Macromolecules* **1990**, *23*, 1821.
(63) Coviello, T.; Burchard, W.; Geissler, E.; Maier, D. *Macromolecules* **1997**, *30*, 2008.
(64) Chevillard, C.; Axelos, M. A. V. *Colloid Polym. Sci.* **1997**, *275*, 537.
(65) Sarkar, N. *J. Appl. Polym. Sci.* **1979**, *24*, 1073.
(66) Sarkar, N.; Walker, L. C. *Carbohydr. Polym.* **1995**, *27*, 177.
(67) McCrystal, C. B.; Ford, J. L.; Rajabi-Siahboomi, A. R. *J. Pharm. Sci.* **1999**, *88*, 797.
(68) Velazquez, G.; Herrera-Gómez, A.; Martín-Polo, M. O. *J. Food Eng.* **2003**, *59*, 79.
(69) Fechner, P. M.; Wartewig, S.; Kiesow, A.; Heilmann, A.; Kleinebudde, P.; Neubert, R. H. H. *J. Pharm. Pharmacol.* **2005**, *57*, 689.
(70) Lin, S.-Y.; Wang, S.-L.; Wei, Y.-S.; Li, M.-J. *Surf. Sci.* **2007**, *601*, 781.
(71) Buslov, D. K.; Sushko, N. I.; Tretinnikov, O. N. *J. Appl. Spectrosc.* **2008**, *75*, 514.
(72) Higuera, A.; Bellantone, R. A. *Carbohydr. Polym.* **2010**, *81*, 578.